Received: 8 August 2024 | Accepted: 17 August 2024

DOI: 10.1111/srt.70039

ORIGINAL ARTICLE

WILEY

Quantitative interpretation of infrared images of lower limbs in individuals with and without type 2 diabetes mellitus

Edgar I. Fuentes-Oliver[1,2,3] | **Rosalinda Ortiz-Sosa**[1,2] | **Raúl Serrano-Loyola**[4] | **Rebeca Solalinde-Vargas**[4] | **Crescencio García-Segundo**[1,5]

[1]ICAT, Universidad Nacional Autónoma de México, Mexico City, Mexico

[2]Facultad de Ciencias, Universidad Nacional Autónoma de México, Mexico City, Mexico

[3]Posgrado en Ing. Eléctrica: Instrumentación, Universidad Nacional Autónoma de México, Mexico City, Mexico

[4]Servicio de Cirugía Vascular y Angiología, Hospital General de México, Mexico City, Mexico

[5]Institute of Biological and Medical Imaging, Helmholtz Zentrum, München, Germany

Correspondence
Rosalinda Ortiz-Sosa, ICAT, Universidad Nacional Autónoma de México. Circuito Exterior S/N, Ciudad Universitaria, Mexico City, 04510, CDMX, Mexico.
Email: rosalinda.ortiz@icat.unam.mx

Funding information
Universidad Naconal Autónoma de México, Grant/Award Number: PAPIIT-UNAM IG100821

Abstract

Background: The quantitative interpretation of the radiometric information extracted from infrared (IR) images in individuals with and without type 2 diabetes mellitus (DM2) is an open problem yet to be solved. This is of particular value given that DM2 is a worldwide health problem and onset for evolution toward diabetic foot disease (DFD). Since DM2 causes changes at the vascular and neurological levels, the metabolic heat distribution on the outer skin is modified as a consequence of such alterations. Of particular interest in this contribution are those alterations displayed over the skin's heat patterns at the lower limbs. At the core of such alterations is the deterioration of the vascular and neurological networks responsible for procuring systemic thermoregulation. It is within this context that IR imaging is introduced as a likely aiding tool to assist with the clinical diagnosis of DM2 at stages early enough to prevent the evolution of the DFD.

Methods: IR images of lower limbs are acquired from a cohort of individuals clinically diagnosed with and without DM2. Additional inclusion criteria for patients are to be free from any visible wound or tissue-related trauma (e.g., injuries, edema, and so forth), and also free from non-metabolic comorbidities. All images and data are equally processed and analyzed using indices that evaluate the spatial and temporal evolution of temperature distribution in lower limbs. We studied the temporal response of individuals' legs after inducing an external stimulus. For this purpose, we combine the information of the asymmetry and thermal response index (ATR) and the thermal response index (TRI), computed using images at different times, improving the results previously obtained individually with ATR and TRI.

Results: A novel representation of the information extracted from IR images of the lower limbs in individuals with and without DM2 is presented. This representation was built using the ATR and TRI indices for the anterior and posterior views (PVs), individually and combining the information from both views. In all cases, the information of each index and each view presents linearity properties that allow said information to be interpreted quantitatively in a well-defined and limited space. This representation,

built in a polar coordinate space, allows obtaining sensitivity values of 86%, 97%, and 97%, and specificity values of 83%, 72%, and 78% for the anterior view (AV), the PV, and the combined views, respectively. Additionally, it was observed that the angular variable that defines this new representation space allows to significantly ($p < 0.01$) differentiate the groups, while correlating with clinical variables of interest, such as glucose and glycated hemoglobin.

Conclusion: The linearity properties that exist between the ATR and TRI indices allow a quantitative interpretation of the information extracted from IR images of the lower extremities of individuals with and without DM2, and allow the construction of a representation space that eliminates possible ambiguities in the interpretation, while simplifying it, making it accessible for clinical use.

KEYWORDS
biomedical infrared imaging, diabetes mellitus type 2, diabetic foot disease

1 | INTRODUCTION

Type 2 diabetes mellitus (DM2) is a human-made noncontagious chronic disease that refers to a group of metabolic disorders, where altered physiology takes over, with a consequent biological imbalance of metabolic functions.[1,2] The progression of DM2 over the long term, generally years, is silent, and it causes being diagnosed at advanced stages, where additional comorbidities are present: imbalance in sugar regulation, deficit in insulin production, diabetic neuropathy, and diabetic vasculopathy. Deep down those are expressions of systemic damage that lead to chronic kidney disease, liver dysfunction, diabetic retinopathy, heart disease, and diabetic foot disease (DFD).[3,4]

The silent evolution of the disease is such that when diagnosed, there are advanced stages of systemic inflammation in the vascular and neurological networks. These networks are the main framework of the so-called metabolic heat, a feature that can be physically pictured and even theoretically modeled.[1,5–8]

Due to metabolic processes, the trunk of the human body behaves as a heat source. This can be pictured through infrared (IR) imaging devices—the so-called IR cameras. These images are characteristic heat pattern distributions, which in itself can be assumed as a fingerprint-like of the metabolic performance in each individual. When metabolic disorders arise, the natural metabolic heat distribution is altered, carrying information about the sort of dominant metabolic disorder.[1,2,5] This information is expressed in terms of metabolic heat alterations, which, when pictured as IR images, are a source of anomalous pattern distributions. This signifies that the progression of the metabolic disorder forces the initial heat distribution to drift away from what one can identify as the healthy, or initial, stage of heat distribution.[8–22]

There is an ongoing difficulty in succeeding with establishing a benchmark of the healthy, or initial, stage of heat distribution in a given individual. The ideal scenario is where such sort of distribution is pictured and then set it up as a baseline for grading the drift of the metabolic heat drift. As noted before, the metabolic heat distribution of each individual is unique. Thus, the ideal situation is far from realistic.

This contribution is centered on introducing a self-referencing methodology, along with numerical and graphical tools specifically dedicated to overcoming the difficulty noted in the previous paragraph. By nature, the human body expresses contralateral thermal asymmetry.[18,23–25] It means that human physiology attains equilibrium conditions, and thus the natural asymmetry is a natural initial equilibrium condition. Then when this asymmetry is temporarily challenged by a controlled external thermal stimulus, the measurement of the contralateral asymmetry and its derived relationships would be used as a sort of scale to estimate the drift away from the initial, or healthy, stage.[19,26,27] According to Ortiz-Sosa et al.,[19] both asymmetric and temporal changes due to DM2 can be characterized using a parametric index named asymmetry and thermal response index (ATR). On the other hand, Fuentes-Oliver et al.,[18] pursued the assessment of this issue by using several nonparametric indices related to the thermal asymmetry and the thermal performance of lower limbs after a short-time stimulus is applied. As a result, they introduced the so-called thermal response index (TRI).

Each one of these two indices provides us with different scopes of information in an individual way, which, at the same time, are complementary to each other. Departing from this premise, the core of the present work is to show the simultaneous representation of both indices. The gain in following this pathway is to reinforce the indices of mutual capabilities and emerging properties these have by nature of construction. That is to say, ATR and TRI indices, although independent from each other, have analogous properties as functions. This is regardless that ATR is parametric in the radiated temperature, while TRI is a nonparametric index.

Here we describe a viable strategy for using the previously mentioned indices, extracted from images of the anterior and posterior view (PV) of the lower legs in a cohort of patients clinically diagnosed with DM2 and without visible expressions of the disease. This is done

TABLE 1 Clinical information of the studied groups.

Group	Age (± SD) (years)	BMI (± SD) (kg/m^2)	Glucose (± SD) (mg/dL)	HbA1c (± SD) (%)
Patients with DM2	58.8 (± 9.2)	28.16 (± 3.43)	161 (± 73)	8.41 (± 2.29)
Control subjects	49.6 (± 8.5)	27.69 (± 3.80)	93 (± 7)	5.61 (± 0.30)

Abbreviations: BMI, body mass index; DM2, type 2 diabetes mellitus; HbA1c, glycated hemoglobin; SD, standard deviation.

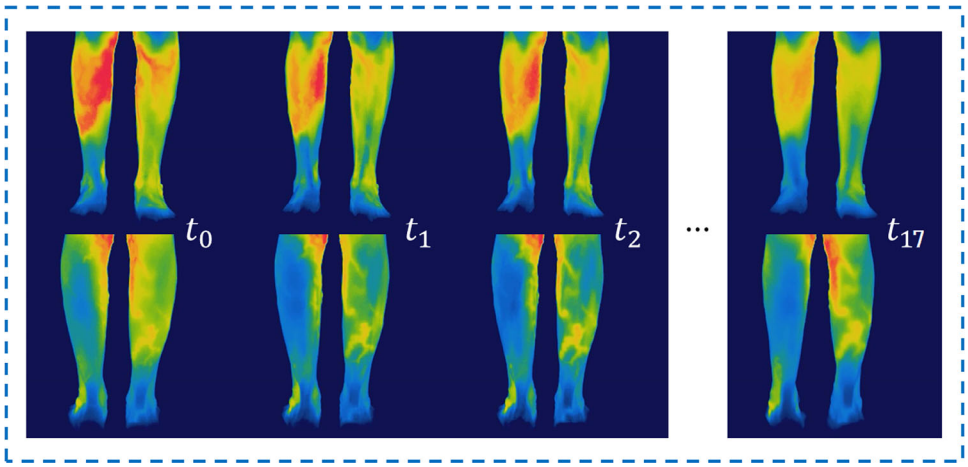

FIGURE 1 IR images acquired from an individual in the studied groups. The upper line corresponds to AV while the bottom line shows images of the PV. From left to right, IR images account for the baseline state (t_0), the time immediately after stimulation, t_1, the time 15 s after the stimulus was applied, t_2, and the time 4 min after stimulation, t_{18}. AV, anterior view; IR, infrared; PV, posterior view.

alongside with its comparison respect equivalent data obtained from a cohort of controls, clinically diagnosed free from the DM2 disease. The method we describe takes into account the combined values of these indices, aiming to obtain a better diagnostic performance. With this methodology, we extract quantitative information from the IR images, and given the mathematical framework and the nature of the extracted information, we manage to establish linearly independent dominions of representation of the information. In the current report, we use the *x*-axis for the TRI and the *y*-axis for the index of ATR, as shown later. In this manner, we manage to overcome the necessity for an external reference, and at once one can get independent quantitative information for each individual. Which compared between healthy and non-healthy, the expectation is to get distinctive differences among the related groups. In summary, the main result we get is this confirmation that meaningful quantitative sets of data related to cross entropy and radiometric information are feasible to obtain and these are unique for each individual. Furthermore, given the nature of these data, those can be represented over a diagram where the patients and controls appear separated, depending upon their asymmetry and thermal performance, which as initially stated, are expected to perform different for patients, respect that for controls.

2 | METHODS

As part of the supervised clinical protocol DI/10/301/4/115 of the General Hospital of Mexico, a set of IR images was acquired from a cohort of 36 patients clinically diagnosed with DM2 and 18 control volunteers without the disease. Laboratory check-ups (blood tests and urinalysis) were done for both groups. Additionally, the clinical record was obtained for the former group by medical staff of the General Hospital of Mexico, after the informed-agreement and signed consent of all the subjects included in the clinical protocol previously mentioned. Some data of interest for both groups can be found in Table 1.

2.1 | Acquisition protocol

IR-images were acquired from the anterior view (AV) and PV of the legs of the subjects. These images were obtained both in passive mode (stand-still position) and in active mode (with an induced thermal stimulus), as shown in Figure 1. The passive mode consists of getting a single image of the legs before the thermal stimulation; that is, the baseline state (t_0). Thermal stimulation was performed by simultaneously cooling both legs using commercial wet wipes. After that, a temporal set of IR images was acquired immediately after the stimulation and then every 15 s for 5 min. This is the active mode acquisition. For the purposes of this work, we only concentrate in a sequence of the first 18 images of the active mode acquisition, that is, the first 4 min after thermal stimulation.

Before the IR-images acquisition, each subject was prepared to uncover the area of interest and rest for 15 min to ensure thermal equilibrium concerning the working environment. In this way, it is possible to minimize the external thermal noise and the thermal fluctuations throughout the study.

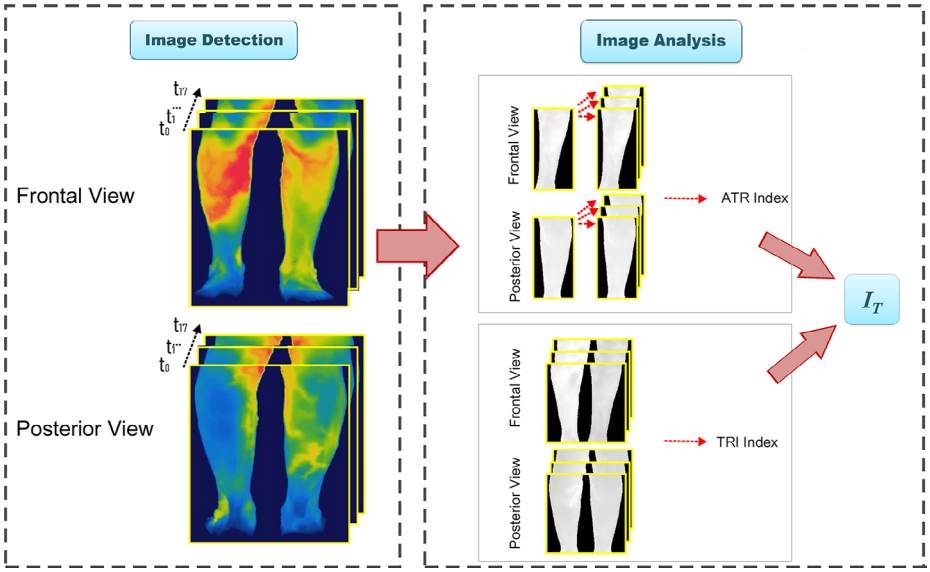

FIGURE 2 General diagram of the IR image acquisition and processing for obtaining ATR and TRI indices. ATR, asymmetry and thermal response index; TRI, thermal response index.

For performing the acquisition, a calibrated IR-camera FLIR-A320 with a thermal sensitivity of 0.05 K was used. This camera was placed in an environment with a controlled temperature set to remain at 20°C, with variations no greater than 1°C while the study was performed. Humidity was continuously monitored as well, remaining always below 60%. The distance was fixed to ensure that the region of interest (ROI), corresponding the o subject's legs, was in the camera's field of view (FOV). Extra details about acquisition protocol are previously reported in refs. [18] and [19].

2.2 | Images analysis

Once the IR images were acquired, cross-entropy (CE) analysis as well as asymmetry analysis were performed for both stand-still and active mode images following the procedure previously described in refs. 18 and 19 The former analysis allows us to get the relative difference between both lower extremities, considering the statistical distribution of temperature as a comparison parameter. For the stand-still images, this relative difference is directly represented through the cross-entropy, and it is later used to compute the ATR, which combines the passive mode information with information about the metabolic evolution of the limbs after stimulation. On the other hand, the asymmetry analysis for the passive mode images results in an index that correlates the thermal information of each limb, looking for the total value of asymmetry between the legs. This index is the thermal asymmetry index (TAI). The TAI is computed not only for the stand-still images but also for the temporal set of images acquired in the active mode, producing a curve that describes the temporal behavior of TAI. Using some characteristics of this curve, a new index, named TRI, is obtained. This TRI describes the temporal behavior of the legs' asymmetry, which is closely related to the metabolic evolution of the limbs after stimulation. A general guide for this process is displayed in Figure 2.

ATR is an index that provides information on metabolic deterioration from numerical values that correspond to both asymmetry and thermal recovery after thermal stimulation. This index, adapted from,[19] is defined as:

$$ATR = \frac{\overline{D}\left(P_{t_2}||P_{t_1}\right)}{\overline{D}\left(P_{R_{t_0}}||P_{L_{t_0}}\right)}; \quad (1)$$

where $\overline{D}(P_{t_2}||P_{t_1})$ is the thermal distance between the state immediately after stimulation and the altered state 15 s after the stimulus was applied. $\overline{D}(P_{R_{t_0}}||P_{L_{t_0}})$ is the thermal asymmetry between the right R_t0 and left L_t0 reference states.

At the same time, the TRI was computed using the procedure reported in. ref. 18 In detail, *TRI* was obtained as follows:

$$TRI = \frac{SD\left(TAI\left(t\right)\right)}{TAI_m} \cdot \frac{TAI_{t_f}}{TAI_{t_0}}. \quad (2)$$

Here, *TAI*(*t*) represents the temporal evolution of the thermal asymmetry index. *SD*(*TAI*(*t*)) is the standard deviation of the time-dependent TAI-index curve, TAI_m is the mean value of *TAI*(*t*), TAI_{t0} is the initial value of *TAI*(*t*), corresponding to the thermal state before the stimulus, that is, the basal state, and TAI_tf accounts for the last recorded value of *TAI*(*t*) after thermal stimulation was applied.

These indices in their original representation allow for evaluation of the global response of the lower extremities, considering both the AV and the PV, obtaining sensitivity and specificity values of 83% for both parameters in the case of *ATR*, and of 86% and 83% for the *TRI*, respectively.

To obtain a differential evaluation of the information provided by both views, in this work the previously described indices (*ATR* and *TRI*), obtained for each acquisition view, were used as coordinates in a space whose information describes the behavior of the thermal asymmetry

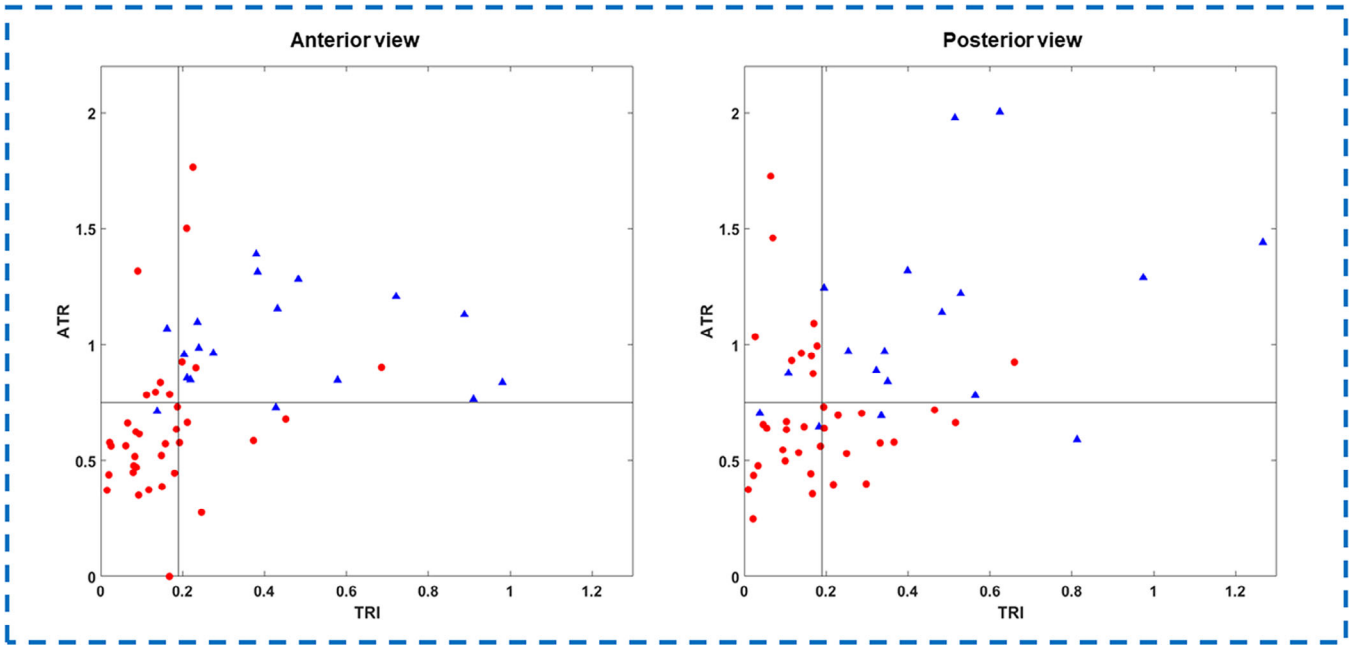

FIGURE 3 ATR and TRI indices behavior for the anterior and PVs. In both graphs, blue triangles correspond to control volunteers, while red circles account for diabetic patients. ATR, asymmetry and thermal response index; PV, posterior view; TRI, thermal response index.

of the lower extremities of an individual in response to an external thermal stimulation. Additionally, the information from both views for each of these indices was combined in such a way that it is possible to retrieve a global representation of the response of the lower extremities, but now in the space described by the *ATR* and the *TRI*. This combined representation was obtained as follows:

$$I_T = \sqrt{I_A^2 + I_P^2}; \tag{3}$$

where I represents any of the indices used in this work (*ATR* or *TRI*), while the subscripts A and P correspond to the anterior and PVs, respectively. Since, in essence, this expression represents the Euclidean distance, and due to the natural equilibrium condition for the asymmetry, this distance has to be bounded. Hence, the relationship between anterior and PVs requires the indices to satisfy linearity conditions. In other words, each pair of indices, anterior and PVs, should fulfill Schwartz's inequality, $|I_{Ai} \cdot I_{Aj} + I_{Pi} \cdot I_{Pj}|^2 \leq |I_{Ai}^2 + I_{Pi}^2 + I_{Aj}^2 + I_{Pj}^2|$; with $i \neq j$. Then this test is carried on as part of the validation process.

These results indicate that the inequality is fulfilled and thus: the indices are bounded, and there exists a linear relationship between each pair of views, for both indices.

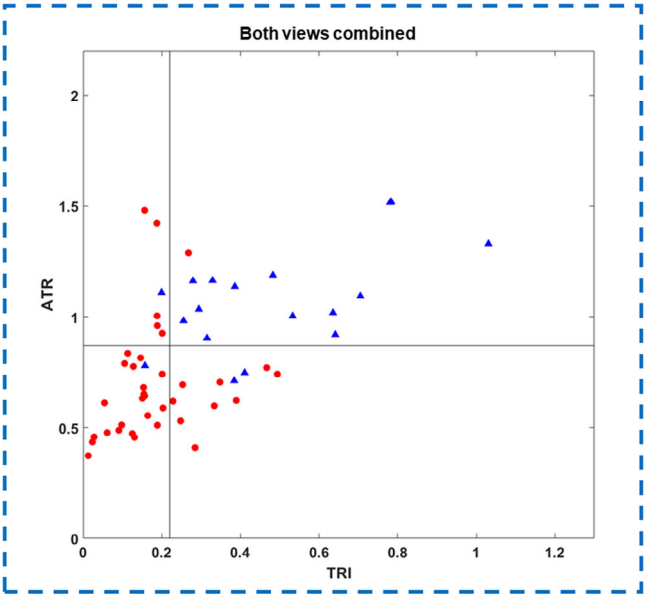

FIGURE 4 ATR and TRI indices behavior for the combination of anterior and PVs. Blue triangles correspond to control volunteers, while red circles account for diabetic patients. ATR, asymmetry and thermal response index; PV, posterior view; TRI, thermal response index.

3 | RESULTS AND DISCUSSION

Figure 3 shows the behavior of the previously described indices for the anterior (Figure 3A) and posterior (Figure 3B) views, respectively. For both views, 0.19 and 0.75 were chosen as threshold values for TRI and ATR, respectively. These thresholds were obtained by maximizing the Youden index, obtaining sensitivity and specificity values of 86% and 83% for the AV, while for the PV, these values were 97% and 72%, respectively.

On the other hand, for the combination of both views (see Figure 4), threshold values of 0.22 and 0.87 were obtained for the TRI and

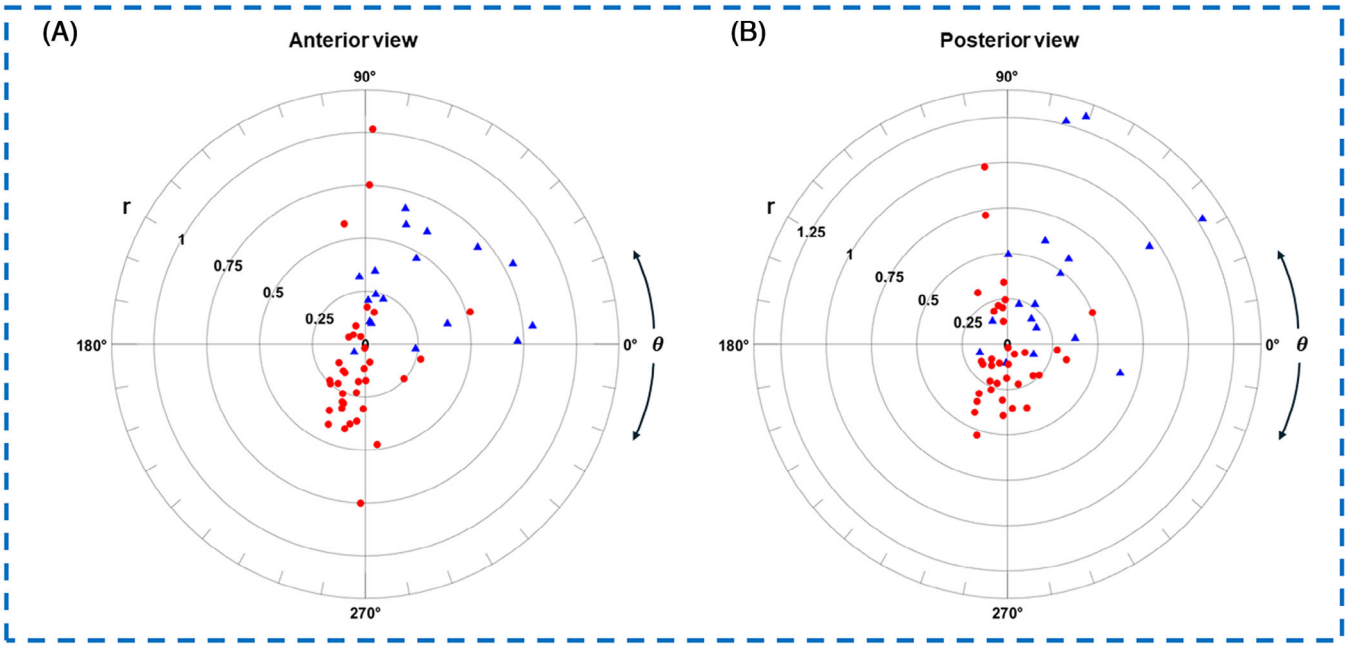

FIGURE 5 Polar representation of the behavior in both groups using the ATR and TRI indices, both for the (A) AV and (B) PV. ATR, asymmetry and thermal response index; AV, anterior view; PV, posterior view; TRI, thermal response index.

ATR indices, respectively. With these thresholds, the sensitivity and specificity obtained were 97% and 78%, respectively.

It should be noted that using these thresholds, it is possible to define four quadrants where the studied subjects are located. In particular, in the upper right quadrant, we find most of the control individuals, while in the lower left quadrant, most of the diabetic patients accumulate.

The quadrant configuration previously shown suggests that a polar representation could provide a more direct interpretation of the results, using the *TRI* and *ATR* indices as the *x*-axis and *y*-axis, respectively. Considering this, we can define the radial and angular coordinates as:

$$r = \sqrt{TRI^2 + ATR^2}; \tag{4}$$

$$\theta = \arctan\left(ATR/TRI\right); \tag{5}$$

In this representation, it is possible to use only the angular coordinate as a parameter to define specific thresholds that are valid not only for the views independently but also for the combined information of both (see Figures 5 and 6). After minding the statistical nature of the indices ATR and TRI, and that the magnitude represented by Equation (4) is again an Euclidean distance, it turns out that the ATR and TRI indices also satisfy Schwartz's inequality: $|TRI_i \cdot TRI_j + ATR_i \cdot ATR|^2 \leq |TRI_i^2 + ATR_i^2 + TRI_i^2 + ATR_j^2|$, with $i \neq j$. This is true for each independent view or by combining the information from both views, as described through Equation (3) and thereafter considerations up to the closing of Section 2. Again, the reason behind checking that this inequality is satisfied is a matter of self-consistency and to show that, besides the construction differences, the magnitude defined by Equation (4), also fulfills linearity conditions within a well-defined and bounded range of values.

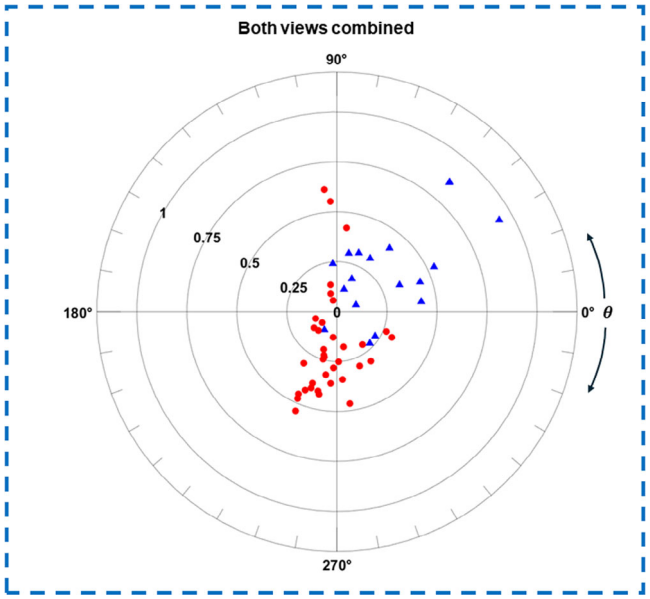

FIGURE 6 Polar representation of the behavior of the studied groups using the ATR and TRI indices for the combined information from both acquisition views. ATR, asymmetry and thermal response index; TRI, thermal response index.

Another advantage of using the angular representation is that it helps to get a simpler and self-explanatory display of the statistical distribution of patients and controls. Since the threshold values defined by the angular coordinate were obtained by maximizing the Youden index for the combined data, then the control individuals tend to be clustered

in the quadrant delimited by the 0° and 90° angles, with ROC-test values for sensitivity and specificity of 86% and 83%, respectively, for the AV. While, for the PV, these values are 97% and 72%, respectively.

Instead, when combining the information carried by both views, the sensitivity and specificity values are 97% and 78%, respectively. It means that the combined sensitivity and specificity produce improved thresholds. Additionally, the extra advantage that polar representation provides is that the same threshold values can be used for each view, when studied independently, and for the combination of both. In this way, the quantitative characteristic of the results becomes unambiguous and the graphical representation assists in simplifying the interpretation and meaning of the results.

As a result of using the polar coordinates representation of the combined information from both views, the specificity of the study is reduced by up to 5% and the sensitivity is increased by up to 14% compared to the results obtained with the ATR and the TRI independently.[18,19] This suggests that the combined information from these indices improves the detection of true positives. Furthermore, from the extracted data, one can visualize that some of the individuals in the control group have some drift toward the non-healthy group, which is the reason for the decrease in specificity. One could hypothesize that these individuals have an ongoing progression toward metabolic disorder, considering that all individuals included in this study, with and without the etiology, were not hand-picked. They were randomly included, provided they fulfilled the inclusion and exclusion criteria.

The hypothesis is supported by the fact that the onset of the DM2 disease and its evolution to DFD are diabetic neuropathy and peripheral vascular disease (PVD).[3,4] The general estimate is that these two pathologies develop nearly simultaneously. Then, as the metabolic damage progresses, one of them dominates the onset of the disease. However, at advanced stages, both etiologies are entangled present. At the macroscopic scale, the damaging effects are the dominant imprint over the metabolic heat distribution. One can recognize that diabetic neuropathy reduces the body's responsiveness to external thermal stimuli, while peripheral vascular disease prompts changes in the vascular network, and hence in the anatomic imprint of the metabolic heat.

The ATR and TRI indices apply in longitudinal and transversal image studies, and in both directions their linearity relationship holds. From the framework of construction of the indices, the dominant part of the ATR index is the longitudinal component, which is presented through the numerator in its definition. Instead, the TRI is more responsive to the cross-sectional component, expressed through the statistical dispersion and average behavior, connected with the Spearman index.

The noted algebraic linearity of the Euclidean magnitudes, or otherwise, distances, is the foremost fundamental property of the ATR and TRI indices and aligns them with the equilibrium property. In biological systems, physiological equilibrium is a fundamental component for regulating and adjusting both the energy consumption and physiological response mechanisms caused by the interaction with the surroundings. Those actions are refereed as homeostasis and allostasis, respectively. Homeostasis relates to the self-regulation process by which biological systems tend to maintain stability while adjusting to optimal conditions for survival. Allostasis refers to the physiological mechanisms or actions that the biological system undergoes to maintain that stability. Both features, by natural principle, should follow a principle of minimum action or lower energy consumption. Ultimately, this means that any alteration the biological system undergoes, it would go through the homeostasis and allostasis mechanisms. From the physical point of view, it means that those processes are deterministic and follow the minimal consumption of the energy principle. This is an essential precondition to ensure the stability and attain the noted biological equilibrium. Mathematically, the Schwartz inequality refers to the minimal trajectory for energy consumption in keeping stability with biological equilibrium. In other words, the ATR and TRI indices are well defined within a continuous and bounded range of values.

As presented in the introduction, diabetic neuropathy, and vasculopathy are the two main branches of macroscopic physiological expression with an imprint over IR imaging. Within this context, one would expect dominant neuropathy the exhibit smaller ATR values as the pathology tends to severity. Instead, when the vasculopathy is the dominant underlying systemic pathology, the TRI values would tend to be smaller values with the increase in severity. The underpinning causal conditions attached to the way the indices are constructed impose the ATR index to be parametric, being the temperature the driven parameter. Under temperature challenge, as the neuropathy progresses, the limbs are less prone to respond to the challenge. The cross-entropy distance between left and right limbs or anterior respect PVs would tend to be smaller. The limbs are less sensitive to stimulus and the thermal differentiation would tend to be null. Instead, TRI is a nonparametric correlation-related index, which measures the statistical dependence between left-to-right views or anterior-to-posterior views. As the severity of the vasculopathy increases, the statistical correlation of one of the limbs shall degenerate earlier concerning its counterpart. In the long run, when the damage is severe, the correlation diminishes and tends to be null.

The noted considerations are introduced as a possible interpretation of the data in Figure 4. The data for patients tend to have increasingly smaller values of both indices, while most of the control volunteers maintain values greater than the specific thresholds. However, some patients present a behavior similar to the controls for a certain index, while for the other index, the values are below the indicated threshold, suggesting that in these patients it is still possible to differentiate which of the two underlying pathologies of DFD is the dominant one. At the same time, some subjects without a clinical diagnosis of diabetes present a closely related behavior with that expected for patients in one of the two indices described in this work, probably implying that these subjects present a metabolic imbalance associated with some degree of pathology that has not yet been diagnosed.

The noted data distributions for both patients and controls are displayed in an analog manner in the Cartesian and the polar representation (see Figure 6). That is to say, the change in representation from Cartesian to polar does not alter the data interpretation. It rather improves and simplifies the interpretation, and at once adds to the benefit that, through the angular coordinate, may well be possible to assess

the dominant factor expressed over the IR images—whether this is nephropathy or vasculopathy, or even both competing. This last statement could be verified over a given patient with longitudinal follow-up for several months.

As a final remark, notice that according to the Mann–Whitney *U*-test, for the Cartesian representation, both indices, the ATR, and the TRI, provide conditions for the studied groups to be significantly differentiated ($p < 0.01$). However, in the case of polar representation, only the angular coordinate grants the possibility for the differentiation to be made significant ($p < 0.01$). Although the radial coordinate does not grant conditions for differentiation, it is better suited for identifying the severity of the physiological alteration or damage.

Similarly, the correlation between ATR and TRI with two characteristic clinical variables of DM2, such as glucose and glycated hemoglobin, is statistically significant ($p < 0.01$); however, the same does not occur in the case of the new variables in the polar representation, where the correlation is not statistically significant. Considering the previous hypothesis that polar representation allows differentiation between subjects with predominantly neuropathy or PVD, this suggests that other clinical variables characteristic of those two underlying pathologies of DFD must be taken into account to make a correlation with the indices in the polar representation and verify if the hypotheses suggested here are true.

4 | CONCLUSIONS

A method to combine ATR and TRI indices as quantitative markers specific to assist in the DM2 clinical diagnosis was introduced. This methodology departed from the extraction of radiometric quantitative information out of IR images of anterior and PVs of human lower limbs. The participants were individuals clinically diagnosed with and without DM2, undergoing inclusion–exclusion criteria, as part of a clinical protocol in the General Hospital of Mexico in Mexico City.

The basis for the construction of these indices was to get quantitative markers related to the natural physiological asymmetry between two biological constituents of the system that are physiologically equivalent, the lower limbs. Although the information was acquired from apparent independent spatial dominions, the systemic performance demands these dominions to react closely simultaneously, maintaining a linear relationship when comparing contralateral and anterior to posterior views. This linearity, along with the continuity and existence of boundary conditions, arose from the fulfillment of the Schwartz inequality. In consequence, this comparison of statistical information extracted from two equivalent, and although independent, spatial heat distributions, leads to the possibility of defining a Euclidean distance and an angle, allowing to graphical display of the defined indices in polar coordinates.

The use of polar coordinates simplifies the interpretation of the information obtained when calculating the ATR and TRI indices for the AV and PV. In either case, the sensitivity and specificity thresholds for both views are above 70%, and when combined the thresholds improve to be above 80% and with satisfactory, $p \leq 0.01$, statistical significance. The best comparison of indices is when combining anterior and posterior views and comparing against the corresponding contralateral view. When the comparison is made individually for each view, it is possible to observe the ongoing trend for each group. Over the combination, this trend is magnified.

The current contribution displays how to overcome the necessity for an external reference, through the extraction of independent quantitative information for anterior and posterior views of the lower limbs of a given individual, within minutes and under controlled environmental conditions. The main result we get is that the obtained indices are unique for each individual and can be followed by comparison, either among individuals or across time for a given individual. Furthermore, the joint display of the indices for patients and controls enhances the underlying physiological alterations imprinted over the metabolic heat distribution pictured from the lower limbs. Such alterations are paramount for the drift of the functional asymmetry and thermal performance, concerning what is expected in the absence of the vascular damage and neuropathy disease, induced by the metabolic alterations associated with the evolution of the DM2 disease.

Finally, the polar representation, at first glance, greatly simplifies the interpretation of the results. The arising question emerging from the current contribution is to question whether is possible to differentiate the dominance of the vascular disease or the diabetic neuropathy, and over the extension for a longitudinal study, one can different degrees of severity, or effectiveness of a given clinical treatment. Indeed, these are open to question to set up specific hypotheses that are yet to be corroborated.

ACKNOWLEDGMENTS

Edgar I. Fuentes-Oliver acknowledges the financial support through a scholarship granted by Mexican Consejo Nacional de Humanidades, Ciencias y Tecnologías (CONAHCYT). Rosalinda Ortiz-Sosa acknowledges the postdoctoral position support at ICAT-UNAM, granted by the State Government of Hidalgo, within the framework of the Consejo de Ciencia, Tecnología e Innovación de Hidalgo (CITNOVA). C. García-Segundo gratefully acknowledges the PASPA-DGAPA program at UNAM for the sabbatical support as a visiting researcher at the Institute of Biological and Medical Imaging, Helmholtz Zen- trum, München, Germany. He also gratefully acknowledges Prof. Frank Filbir for his support as host during the stay. This work was solely founded by the Universidad Naconal Autónoma de México through the grant PAPIIT-UNAM IG100821.

CONFLICT OF INTEREST STATEMENT

All authors declare the nonexistence of competing interests in any material, qualitative, or institutional manner, among themselves and the parent institutions.

DATA AVAILABILITY STATEMENT

The data that support the findings of this study are available on request from the corresponding author. The data are not publicly available due to privacy or ethical restrictions.

ETHICS APPROVAL AND CONSENT TO PARTICIPATE

The protocol of acquisition and analysis of infrared images presented in this work was evaluated and approved by the Ethics Committee of the General Hospital of Mexico (DI/10/301/4/115) and all participants gave written informed consent before enrolment and data collection.

ORCID

Edgar I. Fuentes-Oliver https://orcid.org/0000-0002-6251-9292
Rosalinda Ortiz-Sosa https://orcid.org/0000-0002-8416-3258

REFERENCES

1. Poretsky L. *Principles of Diabetes Mellitus*. Springer; 2010.
2. Hall JE, Guyton AC. *Textbook of Medical Physiology*. Saunders Elsevier; 2011.
3. *Global report on diabetes*. World Health Organization. Accessed January 6, 2024. http://www.who.int/diabetes/global-report/en/
4. *IDF Diabetes Atlas* 10th ed. International Diabetes Federation. 2021. Accessed January 6, 2024. https://diabetesatlas.org//idfawp/resource-files/2021/07/IDF_Atlas_10th_Edition_2021.pdf
5. Blatteis CM, Taylor N, Duncan N. *Thermal Physiology. A Worldwide History*, Springer Nature; 2022.
6. Ring EF, Ammer K. Infrared thermal imaging in medicine. *Physiol Meas*. 2012;33:R33–R46.
7. Diakides M, Bronzino JD, Peterson DR. *Medical Infrared Imaging: Principles and Practices*. CRC Press; 2013.
8. Ring F, Jung A, Żuber J. *Infrared Imaging. A Casebook in Clinical Medicine*. IOP Publishing; 2015.
9. Houghton VJ, Bower VM, Chant DC. Is an increase in skin temperature predictive of neuropathic foot ulceration in people with diabetes? A systematic review and meta-analysis. *J Foot Ankle Res*. 2013;6(1):31.
10. Ammer K. The Glamorgan protocol for recording and evaluation of thermal images of the human body. *Thermol Int*. 2008;18(4):125–144.
11. Zhang WZ, Jiang BY, Ye C, et al. Preliminary study of finger temperature recovery in patients with diabetes mellitus following cold stimulation. Diabetes/metabolism research and reviews. *Diabetes Metab Res Rev*. 2024;40:e3706.
12. Ring EFJ, Ammer K. The technique of infra red imaging in medicine. *Thermol Int*. 2000;10(1):7–14.
13. Sheen YJ, Sheu WH, Wang HC, Chen JP, Sun YH, Chen HM. Assessment of diabetic small-fiber neuropathy by using short-wave infrared hyperspectral imaging. *J Biophotonics*. 2022;15(2):e202100220.
14. Petrova NL, Donaldson NK, Tang W, et al. Infrared thermography and ulcer prevention in the high-risk diabetic foot: data from a single-blind multicentre controlled clinical trial. *Diabet Med*. 2020;37(1):95-104.
15. Cao Z, Zeng Z, Xie J, et al. Diabetic plantar foot segmentation in active thermography using a two-stage adaptive gamma transform and a deep neural network. *Sensors*. 2023;23(20):8511.
16. Faus Camarena M, Izquierdo-Renau M, Julian-Rochina I, Arrébola M, Miralles M. Update on the use of infrared thermography in the early detection of diabetic foot complications: a bibliographic review. *Sensors*. 2023;24(1):252.
17. Godavarty A, Leiva K, Amadi N, Klonoff DC, Armstrong DG. Diabetic foot ulcer imaging: an overview and future directions. *J Diabetes Sci Technol*. 2023;17(6):1662-1675.
18. Fuentes-Oliver EI, García-Segundo C, Solalinde-Vargas R, Ortiz-Sosa R, Serrano-Loyola R. Anomalous contra-lateral radiometric asymmetry in the diabetic patient. *Biomed Phys Eng Express*. 2019;5(6):1–13.
19. Ortiz-Sosa R, Fuentes-Oliver EI, García-Segundo C, Serrano-Loyola R, Solalinde-Vargas R. Analysis of the density and distribution of entropy in biomedical infrared imaging for diabetes mellitus type II. *Biomed Phys Eng Express*. 2021;7(4):10.
20. Ortiz-Sosa R, Fuentes-Oliver EI, García-Segundo C, Serrano-Loyola R, Solalinde-Vargas R. On the stability of asymmetry of thermal emission in diabetic foot disease. *AIP Conf Proc*. 2021;2348:050010.
21. Fuentes-Oliver EI, García-Segundo C, Serrano-Loyola R, Solalinde-Vargas R, Ortiz-Sosa R, Gastélum-Strozzi A. Quantification of thermal asymmetry in diabetic foot disease. *AIP Conf Proc*. 2019;2090:040002.
22. Tang Y, Xu F, Lei P, Li G, Tan Z. Spectral analysis of laser speckle contrast imaging and infrared thermography to assess skin microvascular reactive hyperemia. *Skin Res Technol*. 2023;29:e13308.
23. Liu C, Van der Heijden F, Klein ME, Van Baal JG, Bus SA, Van Netten JJ. Infrared dermal thermography on diabetic feet soles to predict ulcerations: a case study. *Proc. of SPIE*. 2013;8572:85720N.
24. Liu C, Van Netten JJ, van Baal JG, Bus SA, van der Heijden F. Automatic detection of diabetic foot complications with infrared thermography by asymmetric analysis. *J Biomed Opt*. 2015;20(2):026003.
25. Macdonald A, Petrova N, Ainarkar S, et al. Thermal symmetry of healthy feet: a precursor to a thermal study of diabetic feet prior to skin breakdown. *Physiol Meas*. 2017;38(1):33–44.
26. Bharara M, Viswanathan V, Cobb JE. Cold immersion recovery responses in the diabetic foot with neuropathy. *Int Wound J*. 2008;5(4):562–569.
27. Bharara M, Viswanathan V, Cobb JE. Warm immersion recovery test in assessment of diabetic neuropathy—a proof of concept study. *Int Wound J*. 2008;5(4):570–576.

How to cite this article: Fuentes-Oliver EI, Ortiz-Sosa R, Serrano-Loyola R, Solalinde-Vargas R, García-Segundo C. Quantitative interpretation of infrared images of lower limbs in individuals with and without type 2 diabetes mellitus. *Skin Res Technol*. 2024;30:e70039. https://doi.org/10.1111/srt.70039